Characterization of an Intra-Body Wireless Link in the UHF Band

**Fatiha Mghar[1], Antoine Diet[1, *], Chadi Gannouni[1],
Lionel Pichon[1], Olivier Meyer[1], and Stavros Koulouridis[2]**

Abstract—Recent advancement in ultra-low-power electronics and radio communications has significantly contributed to the development of miniaturized biomedical sensors capable of capturing and transmitting wirelessly physiological data. The characterization of signal and power transmission inside the human body is of great importance. This paper investigates the case of an intra-body wireless communication in the UHF frequency band. An implanted antenna (bent dipole) is designed to operate efficiently in a biological tissue model. Predictions of the performances obtained by 3D electromagnetic simulations are compared to measurements in a realistic environment (pork meat in a box of $18 \times 10 \times 7 \, \text{cm}^3$). The antennas show return loss matching of $-12\,\text{dB}$ at $1.2\,\text{GHz}$, in the presence of the meat. Then a characterization of the transmission link between two antennas is performed both numerically and experimentally at $1.2\,\text{GHz}$. At this frequency, the measured $|S_{21}|^2$ is around $-35\,\text{dB}$ at $6\,\text{cm}$, and $-40\,\text{dB}$ at $8\,\text{cm}$. The simulation of the $|S_{21}|^2$ highlights the impact of the conductivity of the tissues, driving to values of -25 to $-55\,\text{dB}$ at $6\,\text{cm}$, and -30 to $-65\,\text{dB}$ at $8\,\text{cm}$. The characterization of the pork meat conductivity is evaluated experimentally around $2\,\text{S/m}$. During the process of characterization, this value may be over-estimated due to the pressure applied on the sample. The simulations results are compared with measurements results, and also with retro-simulations results. The latter are considered as a worst case due to the losses implied by the over-estimated conductivity value.

1. INTRODUCTION

Biomedical implants in human body are used nowadays for various types of constant monitoring (stress, body temperature, glycemic rate,...) and/or for drugs delivery [1–10]. Such kind of medical data recovery is helpful for medium and long-term observation and can play a critical role in the detection of future diseases. In the idea to efficiently monitor the different data without modifying the activity or habits of the patient, a wireless body area network (WBAN), dedicated to the medical implants, is investigated for many years. Several approaches can be found in the literature in which the implants often use antennas for communication between the body and the exterior, e.g., intra-body to out-body communication. At first glance, each implant is supposed to communicate with the exterior by itself [11–14]. In some typical situations where the implants are communicating with each other, intra-body, a single access point may be sufficient for communicating all the collected (in-body) data towards the out-of-body receiver. In [15], the intra-body propagation channel between two implanted antennas was studied in the MedRadio operating band (2.36–$2.40\,\text{GHz}$), highlighting with electromagnetic modeling, the influence of the tissue interfaces. In [16] the case of both ISM $2.45\,\text{GHz}$ and using UWB (Ultra Wide Band) technology was considered and studied thanks to an adequate numerical model. Some in-body to in-body channel modeling was also proposed in [17, 18] for the UWB, but only full-wave models were

involved. In [19], the performance of an implantable folded dipole antenna was evaluated for in-body wireless communication in UHF (Ultra High Frequency, 300 MHz–3 GHz) band; however, only one single antenna was considered, and the link with a receiver was not characterized. The RF intra-body link investigated in this work would be implemented when a requested monitoring is expressed by a node (communicating with out-body reader), driving to successive RF communications between intra-body implants. As a consequence, the implants electronic part of this scenario is an integrated sensor. The need of a battery to feed this sensor and the RF part depends on the power budget link. In this paper, we investigate selected antennas designs for establishing an RF link that may help in the complete system definition.

The principle of a fully intra-body wireless data exchange usually considers the case of a homogenized medium for the modeling of muscle tissue. This hypothesis of homogeneity is frequently used at UHF bands because of the large wavelength (decametric waves) as compared to the size of arteries, veins, blood vessels, nerves, and muscle fiber structure. Implants are expected to be small enough, including the antennas. Reducing the design of UHF antenna to fit into a small volume of a few cm^2 is a first step before miniaturization of the biomedical implant. For establishing a communication between implants, the challenge is to design antennas adapted to the medium and achieve satisfactory wireless power transfer. The power budget link includes the antennas' gain, pathloss, and mismatches losses. The antennas gain can be optimized in a different manner compared to the antenna designed for in-body communication towards the exterior (out-body). The localization of implants is subject to a smaller number of degrees of freedom, when they are implanted into the same arm or leg. Antennas of such a scenario are not required to be omnidirectional, and the range of the communications path length is about several centimeters (less than ten). Improving the directivity of these antennas inside the medium (biological tissue), rather than towards the exterior, is a particular and original key challenge, as seen in Figure 1. The goal of this work is to investigate, in UHF band, the design and validation of a two-antenna system immersed into biological tissue, small enough for being implanted in principle. Each antenna is supposed to be directive to improve the link budget inside the (lossy) biological tissues. This last consideration differs from currently in-body to out-body antennas designed for wireless monitoring and communication systems with implants [1–13] whose antennas radiation patterns typically tend to a radiation in a half-space region. In our scenario, each antenna is protected by a thin and biocompatible coating (to be compliant with medical implants requirements). A comparison between numerical predictions and experimental values of the wireless transmission demonstrates the valuable aspects for the approach and allows to characterize the performances of the communication link between the two implanted antennas.
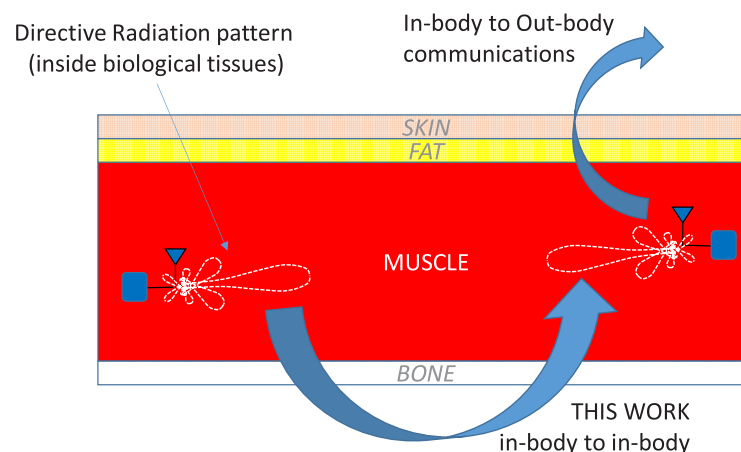

Figure 1. Homogenized model of the in(tra)-body to in(tra)-body wireless link.

Next part of the document presents considerations (buried antennas impedances) and models of the biological tissues. Measurements are performed for evaluating the permittivity and conductivity of the medium in the case of pork meat. The third part presents the design of the antenna adapted to this

medium, and the fourth part summarizes the results and establish a comparison between simulations, measurements, and simulations with the medium characterization (called "retro-simulation"). The last part concludes this work and its perspectives.

2. WAVE PROPAGATION IN BIOLOGICAL TISSUE AND MEDIUM CHARACTERIZATION

The pathloss between the two antennas is determined by the electromagnetic properties of the biological tissues at these frequencies (UHF). Some models, such as Cole-Cole, Debye, are available and used in EM simulations, and numerous experimental works were necessary for evaluating the complex permittivity reference values of the different tissues (skin, fat, muscle, bone, etc.) [20, 21]. Herein, we focused on the muscle tissue. The muscle has a non-neglectable conductivity around $1\,\mathrm{S/m}$ [20, 21].

The mismatch losses are mainly due to the antenna impedance when the antenna is buried into the biological tissue. This impedance is related to the geometry and materials and is highly modified by the presence of the medium (muscle in our context) in the near-field antenna region, especially if the medium has a high relative permittivity and non-zero conductivity. The effect of the relative permittivity was firstly exposed by Deschamps [22], see Equation (1) as a basic knowledge for the case of buried antenna design, well corresponding to our case. In Equation (1), Z and Z_0 are respectively the impedances of the antenna buried and in free space; ω corresponds to the pulsation; ε is the permittivity of the medium in which the antenna is buried; and n is the medium index.

$$Z\left(\omega, \varepsilon, \mu_0\right) = \frac{1}{n} Z_0\left(n\omega, \varepsilon_0, \mu_0\right) \tag{1}$$

The dielectric properties of a material are characterized by the complex relative permittivity defined as follows:

$$\hat{\varepsilon} = \varepsilon' - j\varepsilon'' \tag{2}$$

where ε' and ε'' are the real and imaginary parts of the complex relative permittivity $\hat{\varepsilon}$, respectively.

In this work, the expression of relative permittivity, known as Cole-Cole expression, is used:

$$\hat{\varepsilon}\left(\omega\right) = \varepsilon_\infty + \frac{\varepsilon_s - \varepsilon_\infty}{1 + (j\omega\tau)^{1-\alpha}} + \frac{\sigma_l}{j\omega\varepsilon_0} \tag{3}$$

where ε_∞ and ε_s are the permittivity when $\omega\tau \gg 1$ and $\omega\tau \ll 1$, respectively; α is a measure of the broadening of the dispersion; σ_l is the conductivity due to ionic drift and to the polarization mechanisms at lower frequency; and τ is the mean relaxation time. The Cole-Cole expression in (3) indicates that the dielectric properties of tissues depend on the frequency. The complex permittivity can be expressed with the relative permittivity ε_r and conductivity σ to characterize tissue properties. In this case (2) becomes (4):

$$\hat{\varepsilon} = \varepsilon_r - j\frac{\sigma}{\omega\varepsilon_0} \tag{4}$$

When designing the antenna in this work, the medium is supposed to surround our system, as can be seen in Figure 3.
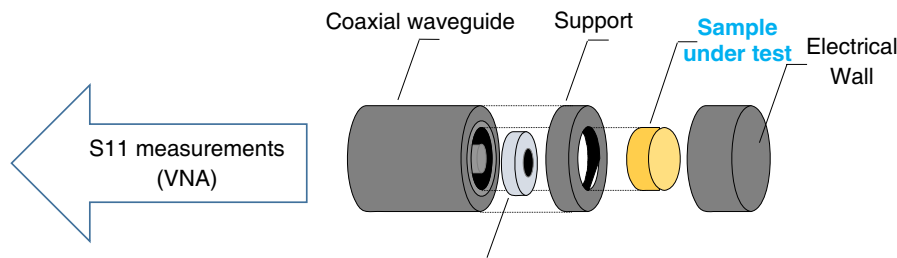

Figure 2. Characterization method used in [31–33]. The sample under test is replaced by a sample of meat in our context.
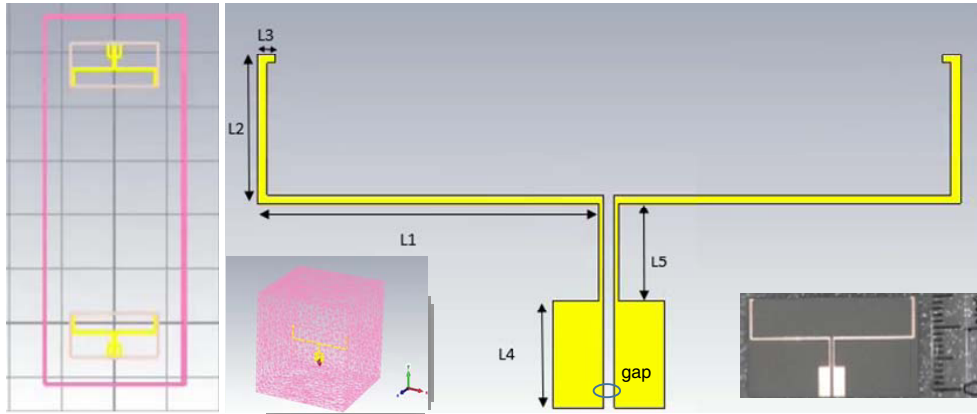
Figure 3. Design of the antenna (corresponding dimensions given in table) after parameterized simulations under CST (left and corner left). Photography (corner right) of the realization on ROGERS 3010 by laser engraving.
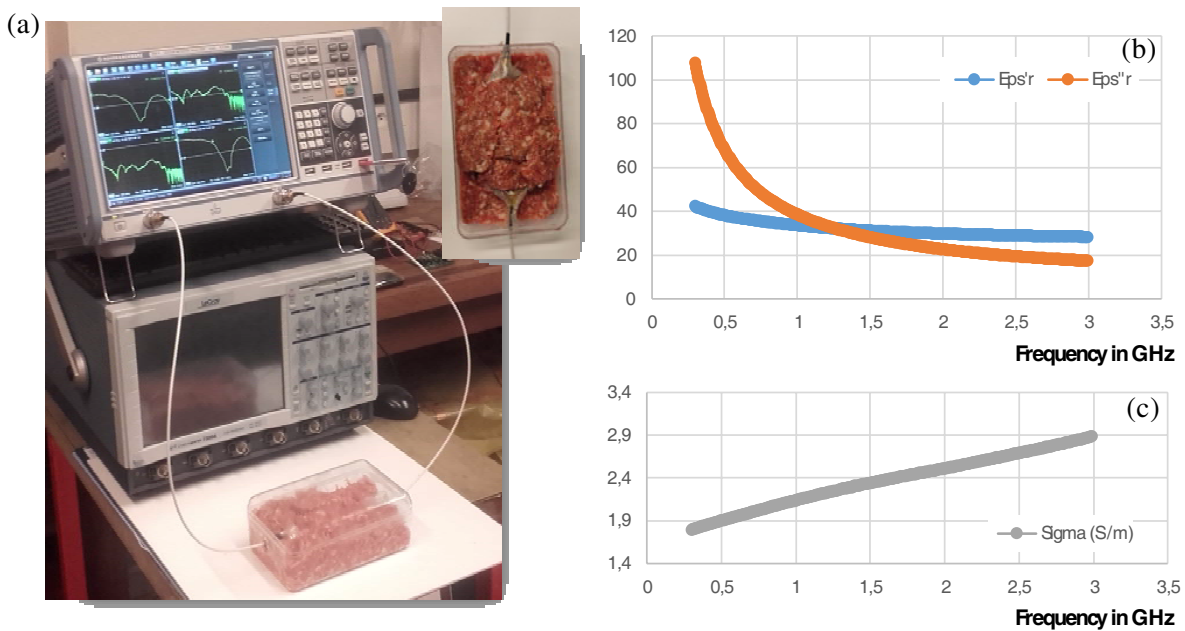

Figure 4. (a) Photography of the measurement setup with the VNA when the antennae are buried in the meat. Characterization measurements of the used meat: (b) complex relative permittivity value in function of the frequency and (c) extraction of the conductivity value in S/m.

To mimic a realistic biological environment, pork meat was chosen for burying the antenna during the S-parameters measurements [25]. The pork meat was included in a plastic box ($18 \times 10 \times 7\,\text{cm}^3$) large enough to consider the same volume of muscle as the homogenized medium of the simulation under CST (Figure 3). A characterization of the pork meat is performed thanks to reflectometry and coaxial cell measurements available in the laboratory [26]. The principle of this method, demonstrated and used in [31–33], is illustrated in Figure 2. From the measured value of permittivity, a "retro-simulation" of the antenna is performed by including the measurements of the pork meat permittivity and conductivity into CST.

The characterization values (permittivity and conductivity) of the meat by reflectometry are reported in Figure 4, in which the permittivity (real and imaginary) and conductivity are plotted versus the frequency. At 1 GHz, the real part of the permittivity is a bit lower, below 40, than expected in the

bibliography giving a typical value of 50 to 55. This shift causes the antenna to be resonant to a slightly higher frequency than expected in the design. Concerning the conductivity, the value is very high, in the range of $2\,S/m$, twice the value expected in the literature. This can be partially explained by the fact that the reflectometry uses a very dense sample, see Figure 2, to the contrary of the measurements in which the meat is not pressed. The density variation may reduce the conductivity in practice.

3. ANTENNA DESIGN

The implanted antenna design was started from a simple half-wavelength dipole model. The coating is Polytetrafluoroethylene (PTFE, $\varepsilon_r = 2.1$ and $\tan\delta = 2e-4$) with a thickness of $0.15\,mm$. Substrate ROGERS RT3010 is chosen for its low losses ($\varepsilon_r = 3$ and $\tan\delta = 4e-4$). As the substrate thickness is small ($0.8\,mm$), the influence of the medium (muscle tissue) permittivity is high enough to reduce the length of the antenna. It is mandatory to assimilate that a part of the medium is in the near-field of the antenna and is so considered as a part of the antenna itself as is the case for any surrounded by dielectric material antenna [23]. The antenna design choice and the characterization of the medium are presented in the following paragraphs because it is hard to consider these aspects of the work separately.

As mentioned in the introduction, a directive antenna benefits the wireless transmission link. With the goal to implant the antenna in a limb (arm, leg), the dipole is bent along the longitudinal axis of the member, to be compliant with the direction of the muscle fiber, providing in that manner the highest gain in the direction of the medium (intra-body) rather than towards the exterior (out-body).

The simulations are done with CST MWS in the UHF band from $600\,MHz$ to $3\,GHz$. As the muscle may reach a high permittivity value around 50 [20, 21], parametric simulations were performed to observe the impact on the antenna characteristics. The impedance of the antenna is strongly impacted by the permittivity and, more generally, by the medium. In fact, the permittivity of the medium modifies the impedance of the antenna in a more complex manner than expected by a simple frequency shift, as expressed in Appendix A for the case of a single dipole [24].

Results of the parametric simulations drive us to improve the matching and bandwidth of the antenna around $1\,GHz$. Each radiating element of the bended printed dipole was considered for this parameterization analysis. The final set of (chosen) parameters corresponds to the antenna shown in Figure 3 and listed in the Table 1. This design improvement was achieved after two steps of parametric optimization: Firstly the size reduction due to the high permittivity value of the medium, and secondly the refine parameters optimization when introducing increasingly the conductivity of this medium. Results are in agreement with the equations of [24] for the case of a cylindrical dipole shape, reported in Appendix A. More precisely, the real part of the impedance antenna tends to be lower when the permittivity increases.

Table 1. Corresponding dimensions of the designed antenna.

Dimensions	Length (mm)	Width (mm)
L1	15.25	0.38
L2	6.7	0.45
L3	0.8	0.38
L4	4.81	2.25
L5	4.32	0.25
gap	$L4 + L5$	0.5

The antenna was then realized by laser engraving. A picture before coating is seen in Figure 3. The extracted physical properties from the medium characterization (pork meat) are included in CST for retro-simulations, and the simulation parameters are extended in terms of conductivity values as additional reference cases.

4. INTRA-BODY WIRELESS LINK MEASUREMENTS ANALYSIS

The two realized antennas are covered by PTFE and buried in the pork meat (as if they were inserted in between two layers of meat), as simulated with CST (see Figure 3) and shown in Figure 4(a). Two transmission distances are considered: 6 cm and 8 cm.

4.1. S-Parameters Simulations and Measurements Comparison

The results presented in this section in terms of reflection and transmission coefficients are of three types: (i) simulations under CST with arbitrary values of permittivity and conductivity in the model of the biological tissue, (ii) simulations (denoted as retro-simulations) under CST with the values of permittivity and conductivity obtained by the characterization of the pork meat, and (iii) VNA (Vector Network Analyzer) measurements of the antennas S-parameters buried in the pork meat.

The reflection coefficient, $|S_{11}|$, is shown in Figure 5, and the transmission coefficient, $|S_{12}|$, in Figure 6 (two sub-figures) for both distances of 6 cm and 8 cm between the two antennas.
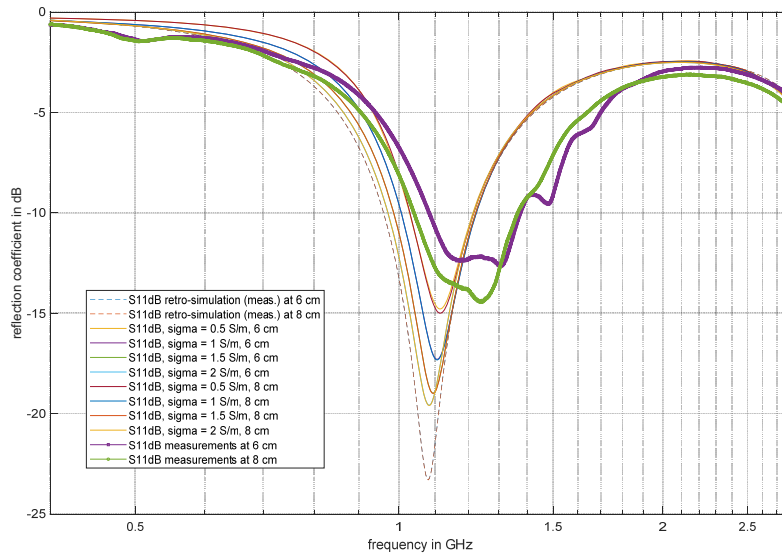

Figure 5. $|S_{11}|$ reflection coefficient (in dB) of the antenna designed at 6 cm and 8 cm distance. Cases are reported (i) for measurements with the VNA, (ii) for CST simulations with a relative permittivity of 40 and a conductivity from 0.5 to 2 S/m, and for (iii) CST retro-simulations including the measured permittivity of the meat (characterization).

As can be seen in Figure 5, the simulation at 6 cm and 8 cm are superposed for the same case of permittivity and conductivity, validating that the antennas do not influence each other (as it could be the case in near field). The variation of the conductivity implies an additional shift in frequency due to the influence of the medium physical properties. Moreover, the conductivity losses lower the reflection coefficient by reducing the reflected power towards the feeding of the antenna, but this is in fact lost power. Finally, the measurements with the VNA show a good agreement with simulation and retro-simulation, in the vicinity of 1.2 GHz.

In Figure 6, the transmission coefficient is shown for the two different distances. It can be noticed in both cases that the retro-simulations results are lower than the measurements. This may be due to the hypothesis that the meat density was not exactly the same during the characterization process, probably because the sample needs to be pressed in a closed volume, for measuring by reflectometry process. When comparing the measurements of the transmission coefficient with the different cases of simulation models, it appears that a value of the conductivity around the 1 S/m seems to match approximately and could result from the presence of air mixed with the pork meat. This value is in
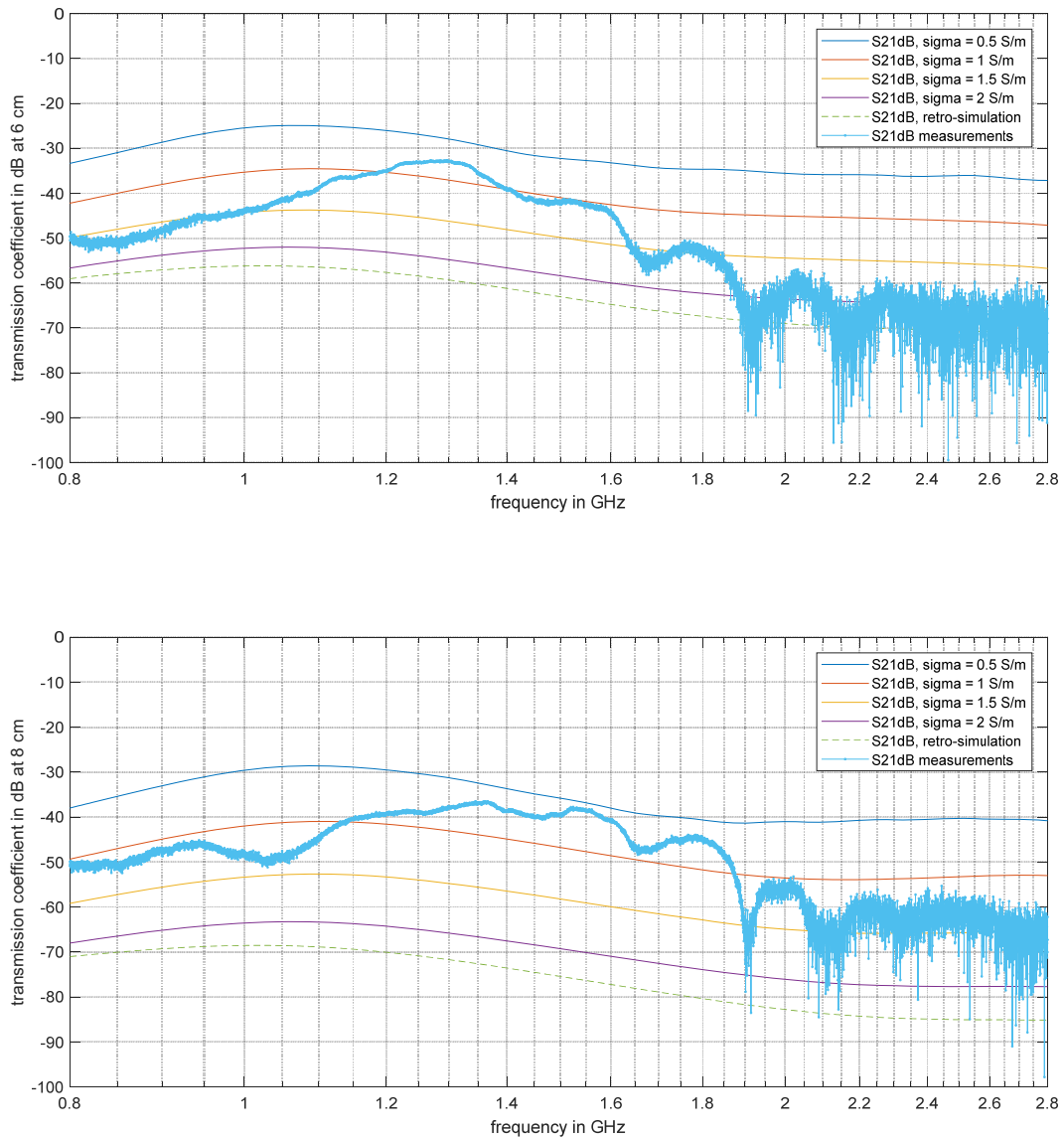
Figure 6. $|S_{21}|$ transmission coefficient (in dB) between the two designed antennae at a distance of 6 cm, top sub-figure, and 8 cm bottom sub-figure. For each of the two sub figures, three results are superposed: (i) measurements with the VNA, (ii) CST simulations with a relative permittivity of 40 and a conductivity from 0.5 to 2 S/m, and (iii) CST retro-simulations including the measured permittivity of the meat.

good agreement with [27]. In Figure 6, the measurements of $|S_{21}|$ seem a bit random in the band 1.9–2.8 GHz, but the corresponding $|S_{11}|$ in Figure 5 indicates that it happens at high return loss (mismatched, around -3 dB) and consequently weakly radiating from the emitting antenna. Taking into account the high losses in the medium, there is very low power that can be received on the port of the VNA in that band of frequency, thus increasing the sensitivity of the measurements to the noise.

This part of our work can be compared with results of [27] in which some simulations and measurements with accurate body models drive to a pathloss, i.e., $|S_{21}|^2$ in dB, in the range of -50 dB at almost 10 cm in the UHF band (300 MHz–3 GHz). Additionally, in [16], the evaluation of the pathloss at 400 MHz (MICS) and 2.45 GHz (ISM) is in the range of 60–80 dB for a distance around 15–20 cm. Table 2 gives more precise comparison of our results with other experiments in the same UHF band.

Table 2. Comparison of the $|S_{21}|^2$ measurements with UHF intra-body published works.

Reference	Frequency band	antenna type	distance	$|S_{21}|^2$
[15]	2.38 GHz	Bow-Tie	8 cm	-70
[27]	0.3–3 GHz	UHF dipole	10 cm	-50 dB
This work	1–1.2 GHz	UHF folded dipole	6 and 8 cm	-35 and -40 dB

4.2. Radiation Pattern

The simulations and measurements of a transmission between two antennas enable to quantify the amount of power that can be expected to flow through the wireless link. The link budget includes the gain of each antenna and the pathloss (path-losses, i.e., $|S_{21}|^2$) of the transmission, but is typically deduced from a free-space model. The pathloss value is mainly linked to the medium characteristics (permittivity, conductivity) and the frequency.

Some complex and parameterized models of pathloss are proposed in the literature for a constrained propagation medium, such as lossy medium or non freespace ones [3, 16, 17, 23, 27]. Herein, we are not considering precise dimension of the medium.

In the link budget, the radiation pattern, i.e., directivity representation in 3D, is used but defined in free space without losses, because the directivity is an antenna property independent from the distance [24, 27, 28]. Herein, the permittivity of the medium has an influence on the calculation of this directivity referred to the air ($\varepsilon_r = 1$). In [29] and [30], the Radiation Pattern (RP) is represented for a given volume of medium modeled by its permittivity. If we introduce some losses due to the conductivity of the medium, the volume in the vicinity of the antenna drives some volume currents and behaves like a radiating element that can be considered as a part of the antenna. It is very difficult to delimit in the space the radiating source which generates the fields, and impossible to consider the directivity property until the distance has an influence on the power calculated (far field hypothesis is not applicable) [28]. Consequently, the radiation patterns are not represented when the medium has losses inside a volume large enough to invalidate the hypothesis of far field propagation.

Figure 7 shows radiation patterns/directivity for finite ($18 \times 10 \times 7$ and $18 \times 10 \times 2$ cm^3) and infinite volumes of the medium with a relative permittivity of $\varepsilon_r = 20$ and 40. Simulations results show that the antenna design is well adapted to permittivity of the medium and present directivity of 2.32 dBi ((a) $\varepsilon_r = 20$) and 2.98 dBi ((b) $\varepsilon_r = 40$). In reality, antennas inside body are close to the limits of the different tissues and limits of the body itself. If the biological tissue is delimited in volume, the background is free space, and the limit of the two media creates waves reflection and transmission in near and far fields. In near field, the consequence is the modification of antennas characteristic such as its directivity (see Figure 7) and reflection coefficient, as show in Figure 7: -7.52 dBi and -5.1 dBi of directivity for the same antenna in two muscle boxes of different heights. In far field, and in our context, multi-paths effects due to the finite volume are present, and highly complexify the evaluation of the pathloss. The conductivity leads to losses that lower the pathloss value towards the level of the measurements values and (retro)simulations shown in Figure 6, in the range of -35 to -40 dB. To summarize, the conductivity of the medium introduces some significant losses but also modifies the equivalent of a complexified radiation pattern of the antenna, including a vicinity with induced current, which must be considered differently for each of the conductivity values.

Table 3 gives the simulations values of Directivities and Gains in the case of the designed antenna in a finite volume of tissue ($17 \times 10 \times 7$ cm^3) with and without introducing the conductivity. As the volume is finite, and the background is free space, as it actually happens, it is difficult to define the radiation pattern of the antenna without including the medium (and its dimensions) present in the near field area of the antenna. The directivity is expressed in dBi and presents very low values because the reference isotropic antenna is in free space. As the losses due to the conductivity impact the efficiency of the antenna because the tissue is in its close vicinity (coating), the gain reported in the Table 3 shows a difference of 4.4 dB compared to directivity. This impact is included in the results of Figure 5 in which the S_{21} is reported.
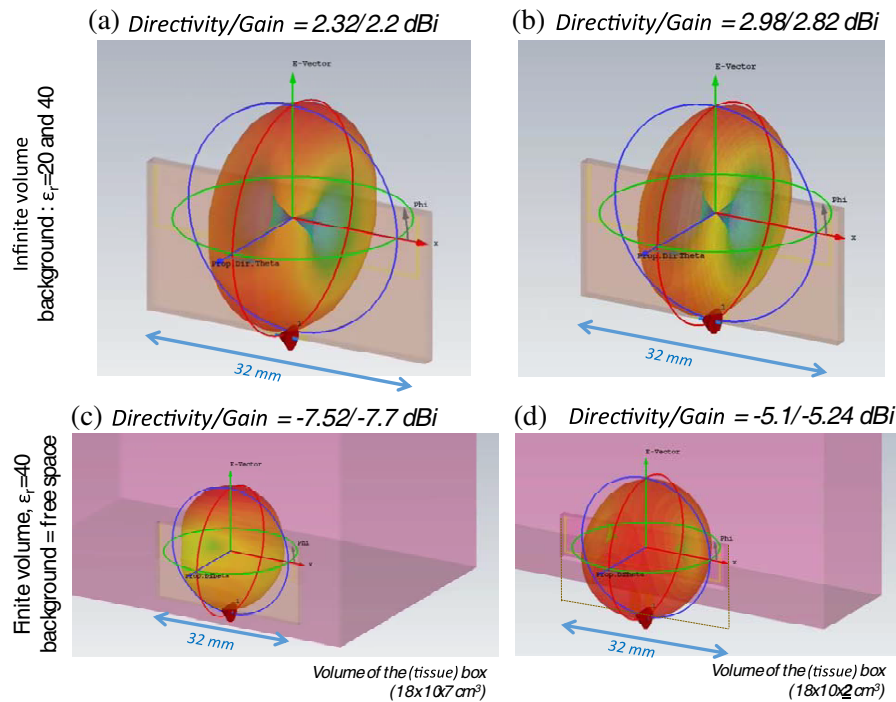
Figure 7. Radiation patterns/directivities and gains of the design antenna in an infinite volume (top sub-figures) for (a) $\varepsilon_r = 20$ and (b) $\varepsilon_r = 40$. Radiation patterns/directivity in free space (bottom sub-figures) with a finite volume (box setup) of biological tissue ($\varepsilon_r = 40$, no losses) of different height, (c) 7 cm and (d) 2 cm.

Table 3. Gain and directivity for the antenna in a finite volume of tissue, with and without conductivity.

	Finite volume ($18 \times 10 \times 7\,\text{cm}^3$) $\varepsilon_r = 40$, $\sigma = 0\,\text{S/m}$ background = free space	Finite volume ($18 \times 10 \times 7\,\text{cm}^3$) $\varepsilon_r = 40$, $\sigma = 1\,\text{S/m}$ background = free space
Gain (dBi)	-5.24	-8.1
Directivity (dBi)	-5.10	-3.7

As can be seen in Figure 8, the current density depends on the conductivity, as expected, which explains qualitatively that the power is concentrated around the emitting antenna. At a given distance, the attenuation is highly affected by the losses, exponentially, as the parameterized simulation has shown. On the other hand, this may reduce a multi-paths effect in a close volume of propagation such as a body arm or leg.

SAR simulations are performed under CST in the case of a lossy medium with a conductivity of $1\,\text{S/m}$, as seen in Figure 9. Medical implants communicate in UHF frequencies at emitted power in the range of microwatts [2, 9, 12, 14]. A limit of $4\,\text{W/kg}$ is allowed by European standards for the arm and legs of human bodies. To establish a limit, the results of Figure 9 correspond to the evaluation by CST of the SAR for an input power of $1\,\text{mW}$. In this figure, it can be seen that the limit of $4\,\text{W/kg}$ is achieved at the vicinity/contact of the metallic part of the antenna. With such a lossy model of $1\,\text{S/m}$, validated by our measurements, it is possible to consider this antenna design for the communication of medical implants.
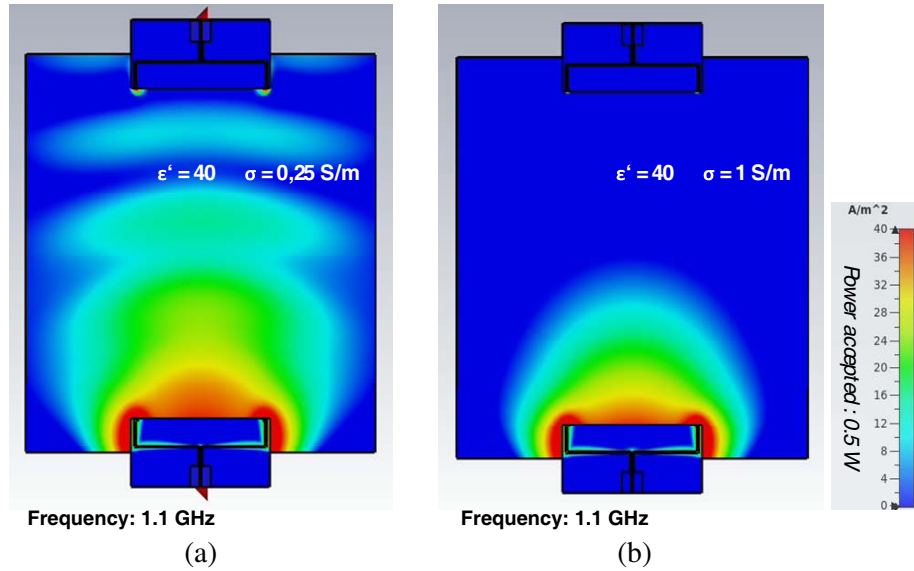
Figure 8. CST simulations results of the designed antenna at 1.1 GHz: RMS current density into the medium for $\varepsilon' = 40$ and (a) $\sigma = 0.25$ S/m and (b) $\sigma = 1$ S/m.
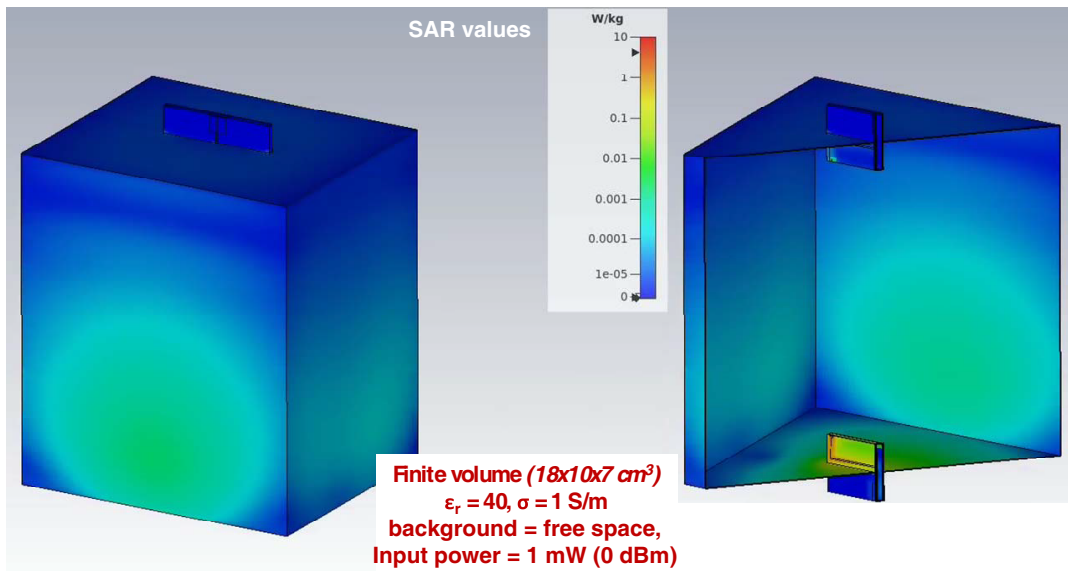

Figure 9. SAR simulations of the antenna in a finite volume $(18 \times 10 \times 7 \text{ cm}^3)$ of lossy medium $(\varepsilon_r = 40, \sigma = 1 \text{ S/m})$ for an input power of 1 mW.

5. CONCLUSION AND PERSPECTIVES

This work showed a simple UHF antenna design, buried in biological tissue and validated by means of VNA measurements in the presence of meat. The originality of this work is that the link is entirely intra-body while lots of state-of-the-art works are focused on the in-body to off-body case, in the same band of frequency (UHF). However, the propagation channel has lots in common in both cases because of the high losses due to the conductivity of the human body tissues, which dominates the pathloss model definition. Concerning the antennas inside the body, in both cases, the high permittivity enables the size reduction of the antenna designed, as the case for buried antenna in underground sensors networks.

The electromagnetic characterization of the meat was discussed and analyzed in simulation and done experimentally in a second step, in order to retro-simulate the measures.

Direct measurements with the VNA were consequently compared with parameterized simulations and with the retro-simulation. The measurements validated the antenna matching (reflection) around 1,2 GHz in the presence of the meat, and the pathloss (transmission) between the antenna at 6 and 8 cm is in the range of −30 dB and −40 dB, respectively. These values are in agreement with results from [10, 27, 29, 30] and complete the state-of-the-art validation of transmission in UHF band over biological tissue. To improve this design, a more directive antenna can be investigated due to the case considered (intra-body) and helped by the finite volume scenario (arm, leg...). Following that idea, directive antennas can be fruitfully positioned.

The reduction of size is potentially possible at 2.4 GHz or 5 GHz, but the conductivity of the muscle may highly increase, and consequently lower the pathloss. As directive antennas can be used for compensating these losses in our context, another dedicated design for quantifying this tradeoff is necessary.

In future designs, the length of the access lines will be increased in order to reduce the potential backward radiation of the antenna (black lobe). Also, directive antennas with an increased ground plane may reduce this potential effect. VNA measurements and radiation patterns also suffer from potentials perturbations due to backward radiations and unbalanced feeding. The transmission coefficient of the RF link investigated may benefit from the design of monopole antennas in future designs.

APPENDIX A. THE IMPEDANCE $Z_M = R_M + X_M$ OF A DIPOLE ANTENNA, OF LENGTH L, IN A MEDIUM OF INDEX N IS

$$
\begin{aligned}
R_m &= \frac{\eta}{2\pi}\left\{ C + \ln(kl) + C_i(kl) + \frac{1}{2}\sin(kl)\left[S_i(2kl) - 2S_i(kl)\right]\right. \\
&\quad \left. + \frac{1}{2}\cos(kl)\left[C + \ln\left(\frac{kl}{2}\right) C_i(2kl) - 2C_i(kl)\right]\right\} \\
X_m &= \frac{\eta}{4\pi}\left\{ 2S_i(kl) + \cos(kl)\left[2S_i(kl) - S_i(2kl)\right] - \sin(kl)\left[2C_i(kl) - C_i(2kl) - C_i\left(\frac{2ka^2}{l}\right)\right]\right\}
\end{aligned}
$$

where:

$$
\begin{aligned}
C &= 0.5772 \,(\text{Euler's constant}) \\
k &= \frac{2\pi}{\lambda} \\
\lambda &= \frac{\lambda_0}{\sqrt{\varepsilon_r}} \\
l &= \frac{\lambda}{2} \\
a &= \frac{\lambda}{1000}, \quad \text{the radius of dipole antenna} \\
\eta &= 120\Pi\sqrt{\frac{1}{\varepsilon_r}}
\end{aligned}
$$

$C_i(x)$ — Cosine integral and $S_i(x)$ — Sine integral.

REFERENCES

1. Agarwal, K., R. Jegadeesan, Y. X. Guo, and N. V. Thakor, "Wireless power transfer strategies for implantable bioelectronics," *IEEE Rev. Biomed Eng.*, Vol. 10, 136–161, 2017, doi: 10.1109/RBME.2017.2683520.

2. Kiourti, A. and K. S. Nikita, "A review of in-body biotelemetry devices: Implantables, ingestibles, and injectables," *IEEE Transactions on Biomedical Engineering*, Vol. 64, No. 7, 1422–1430, Jul. 2017, doi: 10.1109/TBME.2017.2668612.

3. Nikita, K. S., *Handbook of Biomedical Telemetry*, Wiley, IEEE-Press, 2014.

4. Tortora, G., F. Mulana, G. Ciuti, P. Dario, and A. Menciassi, "Inductive-based wireless power recharging system for an innovative endoscopic capsule," *Energies*, Vol. 8, 10315–10334, 2015, https://doi.org/10.3390/en80910315.

5. Kissi, C., et al., "Directive low-band UWB antenna for in-body medical communications," *IEEE Access*, Vol. 7, 149026–149038, 2019, doi: 10.1109/ACCESS.2019.2947057.

6. Kuang, S., G. Yan, and Z. Wang, "Optimization design for receiving coil with novel structure based on mutual coupling model in wireless power transmission for capsule endoscope," *Energies*, Vol. 13, 6460, 2020, https://doi.org/10.3390/en13236460.

7. Rahmat-Samii, Y. and E. Topsaka, *Antenna and Sensor Technologies in Modern Medical Applications*, Wiley, IEEE-Press, 2021.

8. Luu, Q.-T., S. Koulouridis, A. Diet, Y. Le Bihan, and L. Pichon, "Investigation of inductive and radiating energy harvesting for an implanted biotelemetry antenna," *11th European Conf. on Antennas and Propagation (EUCAP)*, Paris, Mar. 20–24, 2017.

9. Shuoliang, D., "Design of a power-efficient radiative wireless system for autonomous biomedical implants," Ph. D. Report, Univ. Paris Saclay, Gif-sur-Yvette, Feb. 5, 2021.

10. Ding, S., S. Koulouridis, and L. Pichon, "Implantable wireless transmission rectenna system for biomedical wireless applications," *IEEE Access*, Vol. 8, 195551–195558, IEEE, 2020, doi: 10.1109/ACCESS.2020.3032848.

11. Wong, K., H. Chang, C. Wang, and S. Wang, "Very-low-profile grounded coplanar waveguide-fed dual-band WLAN slot antenna for on-body antenna application," *IEEE Antennas and Wireless Propagation Letters*, Vol. 19, No. 1, 213–217, Jan. 2020, doi: 10.1109/LAWP.2019.2958961.

12. Sambandam, P., M. Kanagasabai, R. Natarajan, M. G. N. Alsath, and S. Palaniswamy, "Miniaturized button-like WBAN antenna for off-body communication," *IEEE Transactions on Antennas and Propagation*, Vol. 68, No. 7, 5228–5235, Jul. 2020, doi: 10.1109/TAP.2020.2980367.

13. Pei, R., et al., "Wearable belt antenna for body communication networks," *IEEE Antennas and Wireless Propagation Letters*, Vol. 19, No. 12, 2043–2047, Dec. 2020, doi: 10.1109/LAWP.2020.3021677.

14. Benaissa, S., et al., "Propagation-loss characterization for livestock implantables at (433, 868, 1400) MHz," *IEEE Transactions on Antennas and Propagation*, Vol. 69, No. 8, 5166–5170, Aug. 2021, doi: 10.1109/TAP.2021.3060501.

15. El-Saboni, Y., G. A. Conway, and W. G. Scanlon, "Effect of tissue boundaries on the intra-body communication channel at 2.38 GHz," *2017 International Workshop on Antenna Technology: Small Antennas, Innovative Structures, and Applications (iWAT)*, 285–288, 2017, doi: 10.1109/IWAT.2017.7915381.

16. De Santis, V. and M. Feliziani, "Intra-body channel characterization of medical implant devices," *10th International Symposium on Electromagnetic Compatibility*, 816–819, 2011.

17. Fang, X., et al., "Experimental in-body to on-body and in-body to in-body path loss models of planar elliptical ring implanted antenna in the ultra-wide band," *2019 13th International Symposium on Medical Information and Communication Technology (ISMICT)*, 1–5, 2019, doi: 10.1109/ISMICT.2019.8743676.

18. Brumm, J. and G. Bauch, "Verification of a simplified channel modeling technique for ultra wideband in-body communication with simulations," *2020 14th European Conference on Antennas and Propagation (EuCAP)*, 1–5, 2020, doi: 10.23919/EuCAP48036.2020.9135892.

19. Lin, H., M. Takahashi, K. Saito, and K. Ito, "Performance of implantable folded dipole antenna for in-body wireless communication," *IEEE Transactions on Antennas and Propagation*, Vol. 61, No. 3, 1363–1370, Mar. 2013, doi: 10.1109/TAP.2012.2227099.

20. Gabriel, S., R. W. Lau, and C. Gabriel, "The dielectric properties of biological tissues: III. Parametric models for the dielectric spectrum of tissues," *Phys. Med. Biol.*, Vol. 41, No. 11, 2271–2293, Nov. 1996, doi: 10.1088/0031-9155/41/11/003.

21. Bernard, L., "Caractérisation électrique des tissus biologiques et calcul des phénomènes induits dans le corps humain par des champs électromagnétiques de fréquence inférieure au GHz. Modélisation et simulation," fftel00179791v3, Ecole Centrale de Lyon, Universidade federal de Minas Gerais, Français, 2007.

22. Deschamps, G., "Impedance of an antenna in a conducting medium," *IRE Transactions on Antennas and Propagation*, Vol. 10, No. 5, 648–650, Sep. 1962.

23. Zemmour, H., G. Baudoin, and A. Diet, "Soil effects on the underground-to-aboveground communication link in ultrawideband wireless underground sensor networks," *IEEE Antennas and Wireless Propagation Letters*, Vol. 16, 218–221, Institute of Electrical and Electronics Engineers, 2017.

24. Balanis, C. A., *Antenna Theory, Analysis and Design*, 3rd Edition, Wiley Interscience, USA, 2005, ISBN 978-0-471-66782-7.

25. Ngadi, M., S. R. S. Dev, and G. S. Vijaya, "Dielectric properties of pork muscle," *International Journal of Food Properties*, Vol. 18, No. 1, 12–20, 2015, doi: 10.1080/10942912.2010.528112.

26. Belhadj-Tahar, N. E. and A. Fourrier-Lamer, "Broad-band analysis of a coaxial discontinuity used for dielectric measurements," *IEEE Transactions on Microwave Theory and Techniques*, Vol. 34, No. 3, 346–350, 1986.

27. Ibraheem, A. and M. Manteghi, "Intra-body propagation channel investigation using electrically coupled loop antenna," *Progress In Electromagnetics Research M*, Vol. 40, 57–67, 2014.

28. Mirmoosa, M. S., S. Nordebo, and S. A. Tretyakov, "Physical meaning of the dipole radiation resistance in lossless and lossy media," *IEEE Antennas and Propagation Magazine*, Vol. 62, 75–81, 2020.

29. Karlsson, A., "Physical limitations of antennas in a lossy medium," *IEEE Transactions on Antennas and Propagation*, Vol. 52, No. 8, 2027–2033, 2004, https://doi.org/10.1109/TAP.2004.832335.

30. Warren, C. and A. Giannopoulos, "Characterisation of a ground penetrating radar antenna in lossless homogeneous and lossy heterogeneous environments," *Signal Processing*, Vol. 132, 221–226, 2017, ISSN 0165-1684, https://doi.org/10.1016/j.sigpro.2016.04.010.

31. Belhadj-Tahar, N.-E. and A. Fourrier-Lamer, "Broad-band analysis of a coaxial discontinuity used for dielectric measurements," *IEEE Transactions on Microwave Theory and Techniques*, Vol. 34, No. 3, 346–350, 1986.

32. Acikgoz, H., Y. Le Bihan, O. Meyer, and L. Pichon, "Neural networks for broad-band evaluation of complex permittivity using a coaxial discontinuity," *The European Physical Journal Applied Physics*, Vol. 39, No. 2, 197–201, 2007.

33. Meyer, O., C. Gilbert, A. Fourrier-Lamer, and H. Cachet, "In-vitro broad band impedance study of a biochemical reaction under nanopulses: Electrode impedance as a reaction sensor," *Journal of The Electrochemical Society*, Vol. 161, No. 4, B62–B69, 2014.